PPARα/γ Targeting Amorfrutin Phytocannabinoids from Aerial Parts of *Glycyrrhiza foetida*

Elena Serino[†,°], Fabio Arturo Iannotti[‡,°], Hekmat B. Al-Hmadi[§,^], Diego Caprioglio[‖], Claudia Moriello[‡], Francesca Masi[†], Saoussen Hammami[^], Giovanni Appendino[‖], Rosa Maria Vitale[*,‡], and Orazio Taglialatela-Scafati[†,*]

[†]Department of Pharmacy, School of Medicine and Surgery, University of Naples Federico II, Via D. Montesano 49, 80131 Napoli, Italy

[‡]Institute of Biomolecular Chemistry, National Research Council (ICB-CNR), Via Campi Flegrei 34, 80078, Pozzuoli (NA), Italy

[§]Department of Chemistry, College of Medicine, AL-Muthanna University, Samawah, Iraq

[^]Laboratory of Environmental Chemistry and Clean Processes (LR21ES04), Faculty of Sciences of Monastir, Monastir University, Monastir, 5000, Tunisia

[‖]Dipartimento di Scienze del Farmaco, Università del Piemonte Orientale, Largo Donegani 2, 28100, Novara, Italy

[°]These Authors contributed equally to this manuscript

***Corresponding Authors**
(O.T.S.) Tel: +39-081678509; email: scatagli@unina.it,
ORCID: 0000-0001-8010-0180

(R.M.V.) Tel: +39-081-8675316; email: rmvitale@icb.cnr.it
ORCID: 0000-0001-9243-1307

ABSTRACT: A LC-MS/MS guided analysis of the aerial parts of *Glycyrrhiza foetida* afforded novel phenethyl (amorfrutin)- and alkyl (Cannabis)-type phytocannabinoids (six and four compounds, respectively). The structural diversity of the novel amorfrutins was complemented by the isolation of six known members and by the synthesis of analogues edited on the aralkyl moiety. All the compounds so obtained were assayed for agonist activity on PPARα and PPARγ nuclear receptors. Amorfrutin A (**1**) showed the highest agonist activity on PPARγ, amorfrutin H (**7**) targeted selectively PPARα, and amorfrutin E (**4**) behaved as a dual agonist, with the pentyl analogue of amorfrutin A (**11**) being inactive. Decarboxyamorfrutin A (**2**) was cytotoxic and editing its phenethyl moiety to a stiryl or a phenylethynyl group retained this trait, suggesting an alternative biological scenario for these compounds. The putative binding modes of amorfrutins toward PPARα and PPARγ were obtained by a combined approach of molecular docking and molecular dynamics simulations, which provided insights on the structure-activity relationships of this class of compounds.

Phytocannabinoids are biogenetically hybrid natural products based on a polyketide-derived 2,4-dihydroxybenzoic acid core decorated with an isoprenyl unit *para*-oriented to a substituent whose nature mirrors the one of the ketide starter.[1] Thus, pentyl-type phytocannabinoids are derived from an hexanoyl starter, while phenethyl-type phytocannabinoids, never reported from Cannabis, derive from a dihydrocinnamyl starter.[1] As a result of these differences in biogenesis and distribution, phytocannabinoids can be sorted out into alkyl (Cannabis)-type and phenethyl (bibenzyl)-type compounds, exemplified, for non-Cannabis derived compounds, by amorfrutin 2 (**11**) and amorfrutin A (**1**), respectively. Non-cannabis derived phytocannabinoids are known as amorfrutins, and are characterized by a confused, structure-independent and partly overlapping dual semantic of numbers and letters ([A (= 1), B, 2, 3, 4, C, D)]. The archetypal member of this class of compounds is amorfrutin A (**1**), isolated at the beginning of the eighties from the seeds of the bastard indigobush (*Amorpha fruticosa* L.)[2] and from the Australian *Glycyrrhiza acanthocarpa* (Lindl) J. M. Black,[3] both plants belonging to the family Fabaceae (also called Leguminosae). Additional sources of amorfrutins were then identified in South-African *Helichrysum* species, with *H. umbraculigerum* producing both phenethyl- and pentyl phytocannabinoids,[4] in the edible roots of *G. foetida* Desf.[5] from Southern Spain and Northern Africa and in the leaves of the American licorice (*G. lepidota*).[6] On the other hand, amorfrutins have never been isolated from licorice, *G. glabra* L., a well-known medicinal plant and natural flavoring agent.

Initially known only as mild antibacterial agents,[2] amorfrutins then attracted high interest in the wake of the discovery that amorfrutin B (the single analogue embedding a geranyl unit) was a ligand of the transcription factor Peroxisome Proliferator-Activated Receptor γ (PPARγ), and showed potent antidiabetic activity in vivo.[5] Interestingly, amorfrutin A, the deprenyl analogue, showed a reduced (about 1/7) potency compared to amorfrutin B, and a similar decrease in activity was observed for the diprenylated analogue

amorfrutin C (**10**).[5] A crystallographic analysis shed light on the interaction of amorfrutins with PPARγ, whose helix H3 and the β-sheet, placed at the entry side of the ligand binding groove, interact with amorfrutins.[7] This binding mode is distinct from the one of glitazones, and is associated with the activation of a different subset of genes and in a different profile of protein expression, typical of PPARγ partial agonists. Thus, amorfrutins are selective PPARγ activators in white adipose tissue, and improve insulin resistance without the undesirable side effects (including fluid retention, cardiovascular complication, bladder cancer)[5,7] frequently observed with prescribed drugs or other experimental synthetic ligands. Additional targets/activities identified for amorfrutins include the inhibition of the glycolytic enzyme glyceraldehyde 3-phosphate dehydrogenase (GAPDH),[8] involved in neuronal death, of NF-κB and COX, both involved in inflammation,[9] and of the cysteine protease ATG4B,[10] a key regulator of autophagy.

The lack of a systematic phytochemical investigation of *Glycyrrhiza* species, including a detailed characterization of even minor members of the amorfrutin family, and the need for an extension of the structure-activity relationships explored for this class of PPARγ agonists, provided a strong rationale to investigate a Tunisian collection of *G. foetida* (Fabaceae). A preliminary LC-MS analysis of a methanolic extract obtained from the aerial parts revealed an unexpected profligacy of amorfrutin analogues, that were than isolated and structurally characterized. Overall, sixteen amorfrutin derivatives (**1**-**16**), including six new phenylethyl (**4**-**9**) and four new pentyl (**13**-**16**) analogues were obtained. In order to enrich the structural diversity obtained from the natural source, analogues edited on the aralkyl moiety were prepared by synthesis. This library of natural amorfrutins was assayed for agonist activity on PPARα and PPARγ nuclear receptors, discovering a dual agonist activity for compound **4**, a potent and selective PPARα agonist activity for compound **7**, and a significantly increased cytotoxicity for the synthetic analogues bearing unsaturation(s) on

the aralkyl moiety. The molecular bases for these interactions were explored with *in silico* strategy.

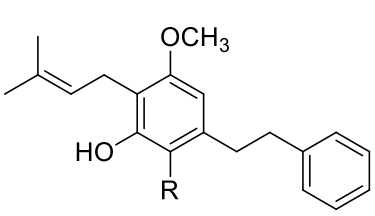

1 R = COOH
2 R = H

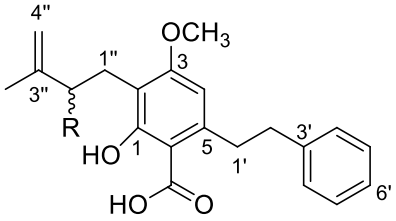

3 R = OH
4 R = OOH

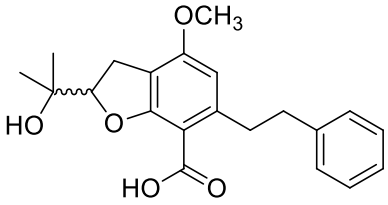

5

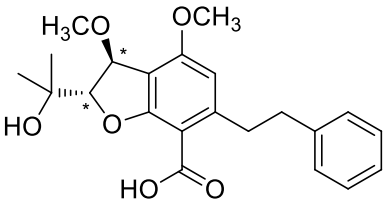

6

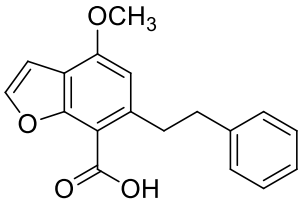

7

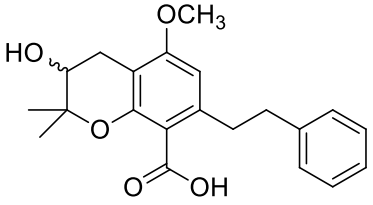

8

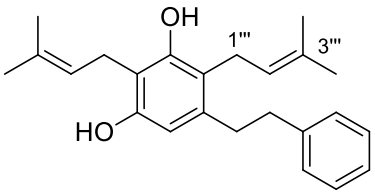

9

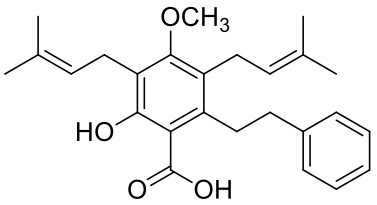

10

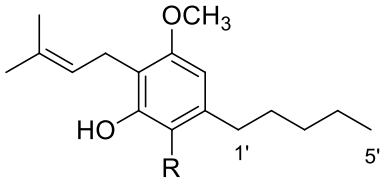

11 R = COOH
12 R = H

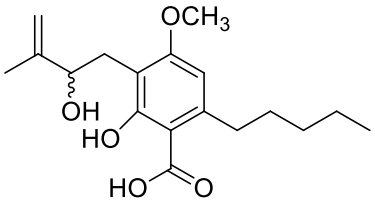

13

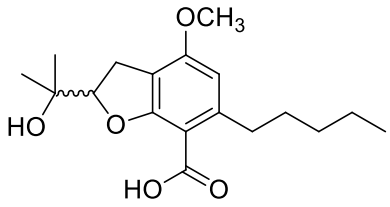

14

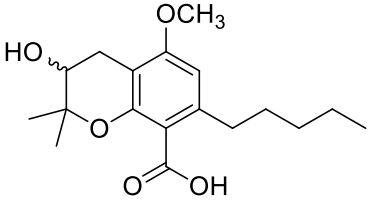

15

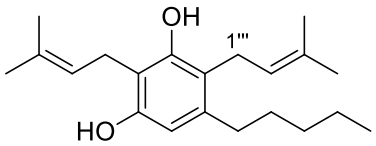

16

Chart 1

RESULTS AND DISCUSSION

Isolation and structural elucidation of amorfrutins. Dried and powdered aerial parts of *G. foetida* were extracted exhaustively with methanol/dichloromethane 1:1. The obtained brown extract was defatted with *n*-hexane, suspended in water and then partitioned sequentially with dichloromethane and butanol. The medium-polarity dichloromethane fraction was analysed via HPLC-mass spectrometry in the positive ion mode, revealing a surprising profligacy of amorfrutin-like compounds (Fig. 1). An accurate manual analysis of the HR-MSMS spectra resulted in the putative identification of some compounds, as reported in Table 1.

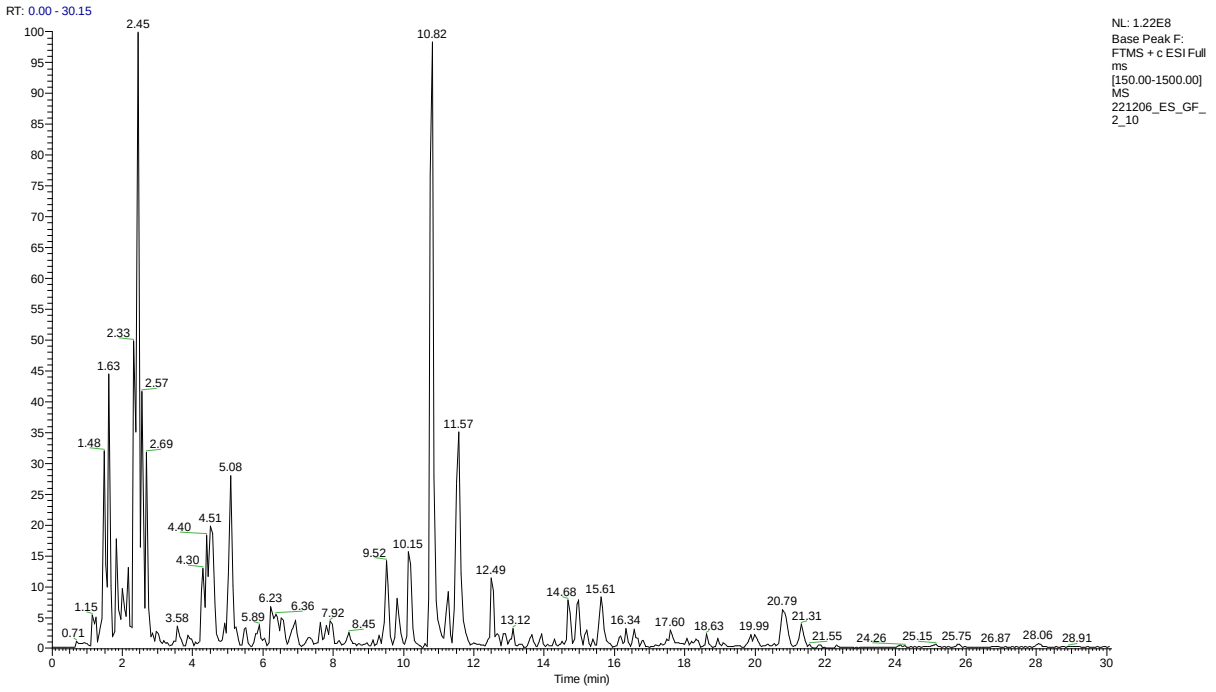

Figure 1. LC-MS chromatogram of the dichloromethane phase of the organic extract obtained from aerial parts of *G. foetida*.

The main component of the mixture (R_t 10.82) was identified as amorfrutin A (**1**) based on its molecular weight (*m/z* 341 $[M+H]^+$), and comparison of the MS/MS fragmentation pattern (Table 1) with literature data.[11] Its decarboxylatyed analogue **2** (R_t 10.15) was also identified, while an additional prominent peak (Rt 11.57) was assigned to the pentyl

analogue amorfrutin 2 (**11**). The peak at R_t 15.61 could be assigned either to a geranylated amorfrutin (e.g. amorfrutin B) or to a bis-isoprenylated amorfrutin (e.g. amorfrutin C). Additional analysis of molecular weights and fragmentation patterns made it possible to confidently identify amorfrutin 3 (**3**) and decarboxyamorfrutin 2 (**12**). None of the other peaks could be assigned by LC/MS analysis, and their characterization required isolation and a detailed NMR spectroscopic investigation.

Table 1. Identified components of the *G. foetida* aerial parts analyzed via LC-MS/MS and some parameters supporting their identification. Compounds are listed in order of LC-MS elution. All mass peaks are $[M+H]^+$ adducts.

Assignment	**Formula**	***R*t (min)**	**Precursor ion (*m/z*)**	**Fragments**
Amorfrutin 3 (**3**)	$C_{21}H_{24}O_5$	2.33	357.16	339.12
Not Assigned	$C_{18}H_{26}O_5$	2.45	323.18	305.17
Not Assigned	$C_{21}H_{24}O_5$	2.57	357.17	-
Not assigned	$C_{18}H_{26}O_5$	2.69	323.18	305.17
Not assigned	$C_{18}H_{16}O_4$	3.58	297.11	279.10, 253.12
Decarboxyamorfrutin A (**2**)	$C_{20}H_{24}O_2$	10.15	297.18	241.12
Amorfrutin A (**1**)	$C_{21}H_{24}O_4$	10.82	341.17	323.16, 285.11
Decarboxyamorfrutin 2 (**12**)	$C_{17}H_{26}O_2$	11.26	263.20	207.13
Not assigned	$C_{24}H_{30}O_2$	11.45	351.23	333.14
Amorfrutin 2 (**11**)	$C_{18}H_{26}O_4$	11.57	307.19	289.17, 251.12
Not Assigned	$C_{21}H_{32}O_2$	12.49	317.24	261.18, 249.18
Amorfrutin C or B	$C_{26}H_{32}O_4$	15.61	409.23	391.22

To this purpose, the dichloromethane phase of the organic extract was purified on a silica gel column eluted with a solvent gradient system based on *n*-hexane/EtOAc mixtures of increasing polarity, followed by repeated HPLC fractionations assisted by the preliminary LC profiling. In this way, 16 amorfrutin-type compounds were obtained in the pure form, including the known amorfrutin A (**1**),[2] its decarboxylated analogue **2**, amorfrutin 3 (**3**),[5] amorfrutin C (**10**),[12] amorfrutin 2 (**11**)[3] and its decarboxylated analogue **12**. The structures

of these known compounds were confirmed by comparison of their chromatographic (LC-HRMS), spectrometric (MS/MS) and spectroscopic (NMR) data with the published ones. The remaining ten compounds were new amorfrutin-type metabolites.

Amorfrutin E (**4**) was isolated as a colorless amorphous solid with molecular formula $C_{21}H_{24}O_6$ (HR-ESIMS). The ^{1}H NMR spectrum of **4** showed typical features of a carboxylated amorfrutin derivative, including the signal of a single aromatic proton (δ_H 6.20) and those of the phenylethyl and the monoterpenyl units. In particular, this latter moiety clearly resembled that of amorfrutin 3 (**3**), but the evident downfield shift of H-2″ (δ_H 4.44) and especially of C-2″ (δ_C 86.5) pointed to the presence of a hydroperoxide group, thus accounting for the additional oxygen atom in the molecular formula. Similarly to amorfrutin 3 (**3**), the molecule was optically inactive and, therefore, racemic.

Amorfrutin F (**5**), an optically inactive compound with molecular formula $C_{21}H_{24}O_5$ (HR-ESIMS), was clearly an analogue of **4** differing only for the functionalization of the terpene moiety, associated to the ^{1}H NMR signals of a deshielded methylene (δ_H 3.12), an oxymethylene (δ_H 4.84) and two methyl singlets. These signals could be accommodated into a dihydrobenzofuran moiety based on the HMBC correlations shown in Figure 2. Particularly important were those from H-2'' to C-1, indicating the presence of the oxygen bridge, and from H_3-4'' and H_3-5'' to C-2''. Thus, structure **5** was assigned to amorfrutin F.

Analysis of ^{1}H and ^{13}C NMR data of amorfrutin G (**6**), $C_{22}H_{26}O_6$ by HR-ESIMS, strongly suggested that this compound was a methoxylated analogue of **5**. Thus, the presence of an additional methoxy group in the ^{1}H NMR spectrum was accompanied by the lack of the methylene H_2-1'', replaced by an oxymethine (δ_H 5.10). Following the association of the proton signals to the resonances of the directly attached carbon atoms, achieved through the HSQC spectrum, the HMBC cross-peaks (Fig. 2) unambiguously indicated the placement of the methoxy group at C-1''. The NOESY correlations of H-1'' with H_3-4''/H_3-5'' and of H-2'' with OMe-1'' indicated the *trans* orientation of the two substituents on the five-

membered ring. Given the absence of optical activity, the compound must be in the racemic form.

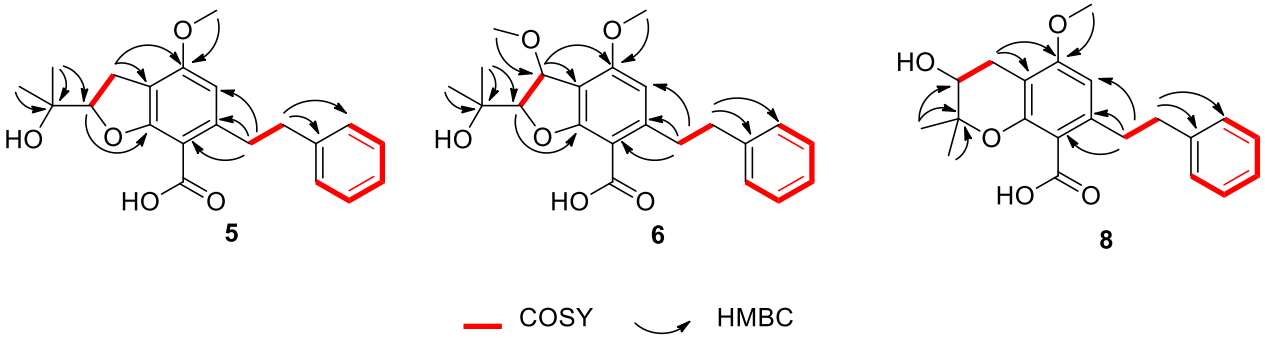

Figure 2. COSY and key HMBC correlations of amorfrutins F (**5**), G (**6**) and I (**8**).

Amorfrutin H (**7**), a colorless amorphous solid with molecular formula $C_{18}H_{16}O_4$ (HR-ESIMS) is characterized by the presence of a benzofurane skeleton, likely derived from the cleavage of the terpene moiety. Its ^{1}H NMR spectrum showed only signals of the phenylethyl moiety, the H-4 singlet of the resorcinol moiety and two broad singlets at δ_H 7.62 and 6.87 that, in agreement with the molecular formula, could be attributed to the furan moiety. The HMBC correlations of H-1'' with C-1, C-2 and C-3 and of H-2'' with C-1 and C-2 secured this structural assignment. This compound has been reported as a synthetic product in a patent,[13] but no NMR data were available for comparison.

The racemic amorfrutin I (**8**), $C_{21}H_{24}O_5$ by HR-ESIMS, shares with amorfrutin F (**5**) the same molecular formula and the phenylethyl resorcinol core, while clear differences in the resonances of the isoprenoid moiety were evident. In particular, the downfield shift of C-3'' (δ_C 80.0) and the upfield shift of H-2'' (from δ_H 4.84 to 3.88) pointed to a hydroxylated chroman-type skeleton. Full NMR assignment was achieved upon inspection of 2D NMR spectra (COSY, HSQC, HMBC) (see Fig. 2).

Compound **9**, $C_{24}H_{30}O_2$ by HR-ESIMS, is a close analogue of the diprenylated amorfrutin C (**10**) lacking the carboxylic group at C-6 ($\delta_{H\text{-}6}$ 6.30) and with an -OH group in

place of the -OMe at C-3. The full NMR assignment of **9** was guided by comparison with data of **10**[12] and inspection of a full set of 2D NMR spectra.

Six amorfrutins of the pentyl type (**11**-**16**) were also isolated. They included the known amorfrutin 2 (**11**) and decarboxyamorfrutin 2 (**12**) and four new analogues (**13**-**16**) embedding terpenoid moieties already detected in the phenethyl analogues.

Amorfrutin J (**13**), $C_{18}H_{26}O_5$ by HR-ESIMS, is the racemic pentyl analogue of amorfrutin 3 (**3**).[5] Accordingly, full NMR assignment based on COSY, HSQC and HMBC spectra indicated that the two compounds differed significantly only for the side chain, with the pentyl H/C signals replacing those of the phenylethyl one. This compound has been mentioned in the proprietary literature as a synthetic derivative, but its NMR data were not available for comparison. Based on the same arguments, we assigned amorfrutin K (**14**) as the pentyl analogue of amorfrutin F (**5**), amorfrutin L (**15**) as the pentyl analogue of amorfrutin I (**8**), and amorfrutin M (**16**) as the pentyl analogue of the diprenylated **9**.

Synthesis of amorfrutin analogues. The structure-activity relationships of amorfrutins have mainly focused on the introduction of substituents on the 3'-phenyl ring and on the homologation of the isoprenyl moiety. The biosynthetic exuberance now detected for *G. foetida* provided the opportunity to investigate the effect of the introduction of oxygen function(s) on the isoprenyl moiety, and we complemented the diversity available by isolation with the synthesis of analogues modified on the two-carbon linker between the two aromatic rings, another unexplored area of the amorfrutin chemical space. Compounds **17-21** (Figure 3) were synthesized to explore the biological space associated with single or double *O*-methylation of the resorcinyl moiety and the introduction of a conjugating unsaturation between the two aryl moieties (Figure 4). Diazotization of 3,5-dimethoxyaniline and treatment with KI, to afford the corresponding iodides, was followed by Sonogashira coupling with phenylacetylene or by Heck coupling with styrene to introduce the C6-C2 moiety at,

respectively, the phenylethynyl or stiryl level, with the ethyl level being obtained by hydrogenation of the ethynyl linker. The isoprenyl moiety was next introduced by lithiation of the aromatic methine adjacent to the two oxygen functions and reaction with prenyl bromide. Given the significant cytotoxicity associated with these compounds (see below), no additional expansion of this preliminary library was carried out.

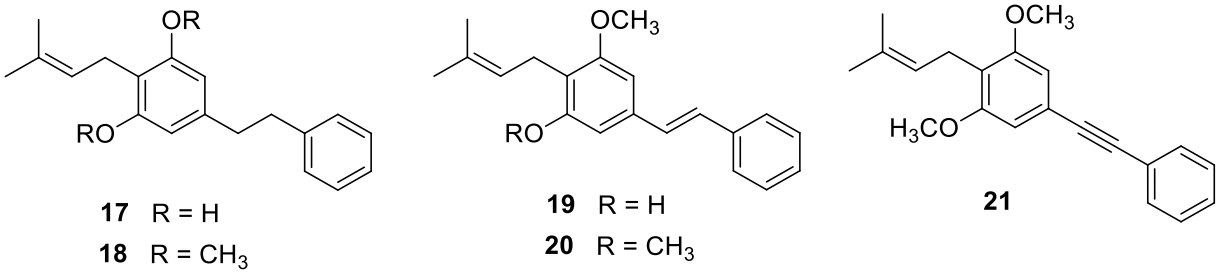

17 R = H
18 R = CH_3

19 R = H
20 R = CH_3

21

Figure 3. Synthetic amorfrutin analogues

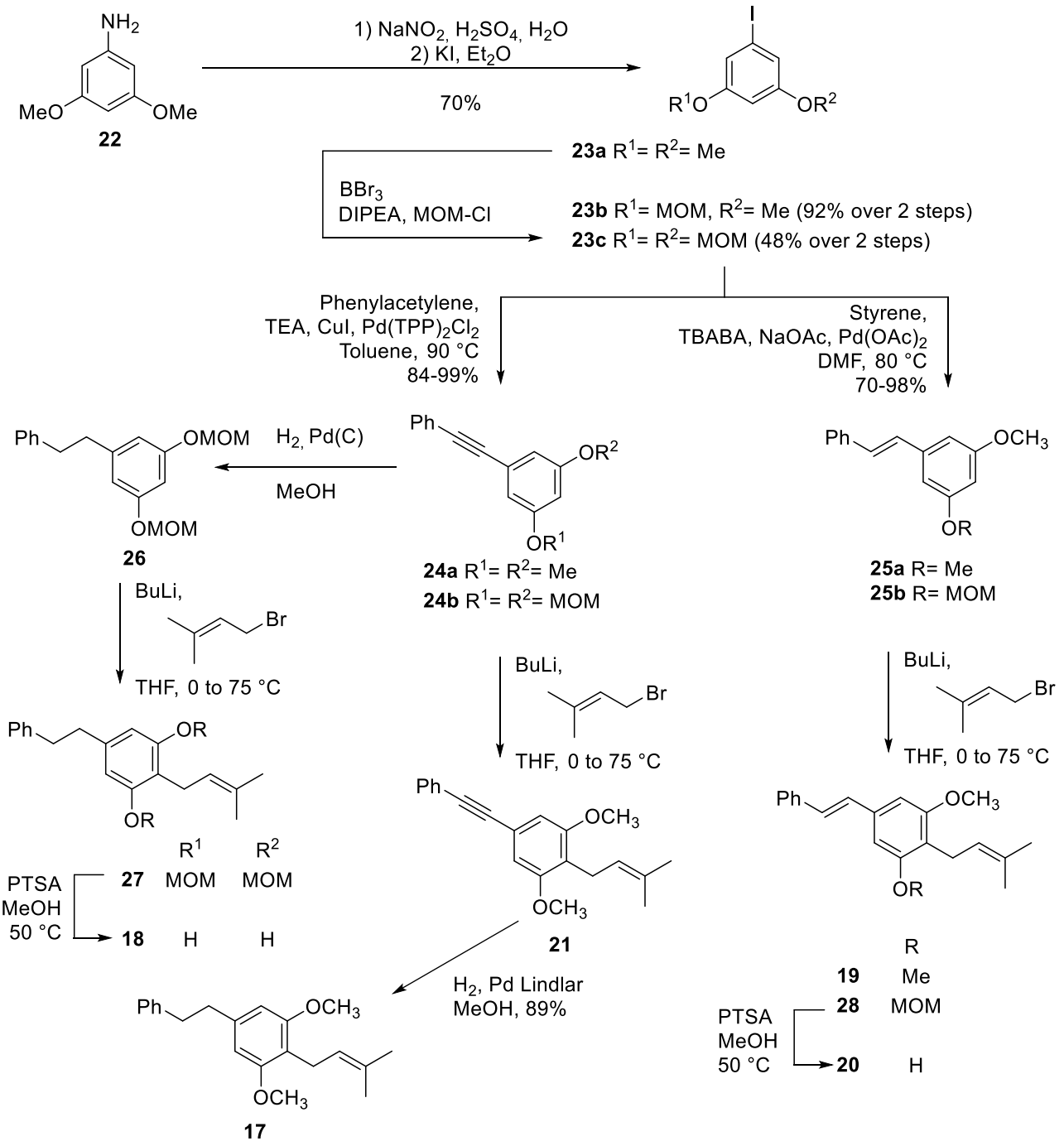

Figure 4. Synthetic scheme for the preparation of amorfrutin analogues

Activity on PPARα and PPARγ. Before testing the potential activity of amorfrutin-like phytocannabinoids on PPARα and PPARγ receptors, their potential toxicity was tested in COS-7 cells, a common fibroblast-like clonal cell line, using the MTT assay. In these experiments, the cells were treated with increasing concentrations of each compound (1, 10, and 30 µM) for 24 hr. As shown in Supplementary Figure S1a-b, a significant cytotoxic

effect was observed with decarboxyamorfrutin A (**2**), its synthetic analogues **17**-**21**, and its *C*-prenyl derivative (**9**), as well as with amorfrutin 2 (**11**). Interestingly, in some cases (e.g. **1** vs. **2** or **9** vs. **10**), the cytotoxic effect appeared to be associated with the lack of the carboxylic group. Based on these results, all compounds showing a cytotoxic effect were excluded from the following experiments. In addition, amorfrutin G (**6**) was not tested because isolated in too small amounts.

COS-7 cells were then used for the luciferase assays. For these experiments, subconfluent cells (60-70%) were transiently transfected with distinct plasmids corresponding to PPARα or PPARγ (ligand binding domain -LBD)/GAL4 (dimerization binding domain –DBD), the UAS enhancer MH100 and Renilla. After transfection, cells were then treated with test compounds at the concentration of 10 µM. The selective agonists GW7647 (0.1 µM, for PPARα) and rosiglitazone (0.1 µM, for PPARγ) were used as control. Fig. 5A shows that amorfrutin A (**1**), amorfrutin 3 (**3**), amorfrutin E (**4**), amorfrutin H (**7**), amorfrutin J (**13**), amorfrutin K (**14**), and amorfrutin M (**16**) significantly promoted PPARα activity (between 5- and 10- fold) compared to vehicle-treated cells. Notably, some of these compounds (**1**, **3**, **4**, **13**) were found also to be active on PPARγ, with amorfrutin A showing the highest effect (fold >20), and with amorfrutin C (**10**) being active only on PPARγ (Fig. 5B). To evaluate more in-depth the dose-response relationship, transfected COS cells were treated with increasing concentrations of the active compounds (0.1 to 30 µM). A linear concentration-response curve (Fig. 5C) for PPARα activation was observed for all compounds except amorfrutin H (**7**), which produced a bell-shaped response, most likely due to the cytotoxic effect observed at the highest concentration (30 µM) (Fig. S1). All compounds showed a linear concentration-response curve also for the activation of PPARγ, plateauing at the two highest concentrations assayed (10 and 30 µM, Fig. 5D).

Taken together, these results show that amorfrutin M (**16**), amorfrutin 3 (**3**), amorfrutin J (**13**) and amorfrutin E (**4**) behave as dual PPARα/γ agonists, amorfrutins C (**10**) and A (**1**) are more potent as PPARγ agonists, while amorfrutin H (**7**) is a selective PPARα agonist.

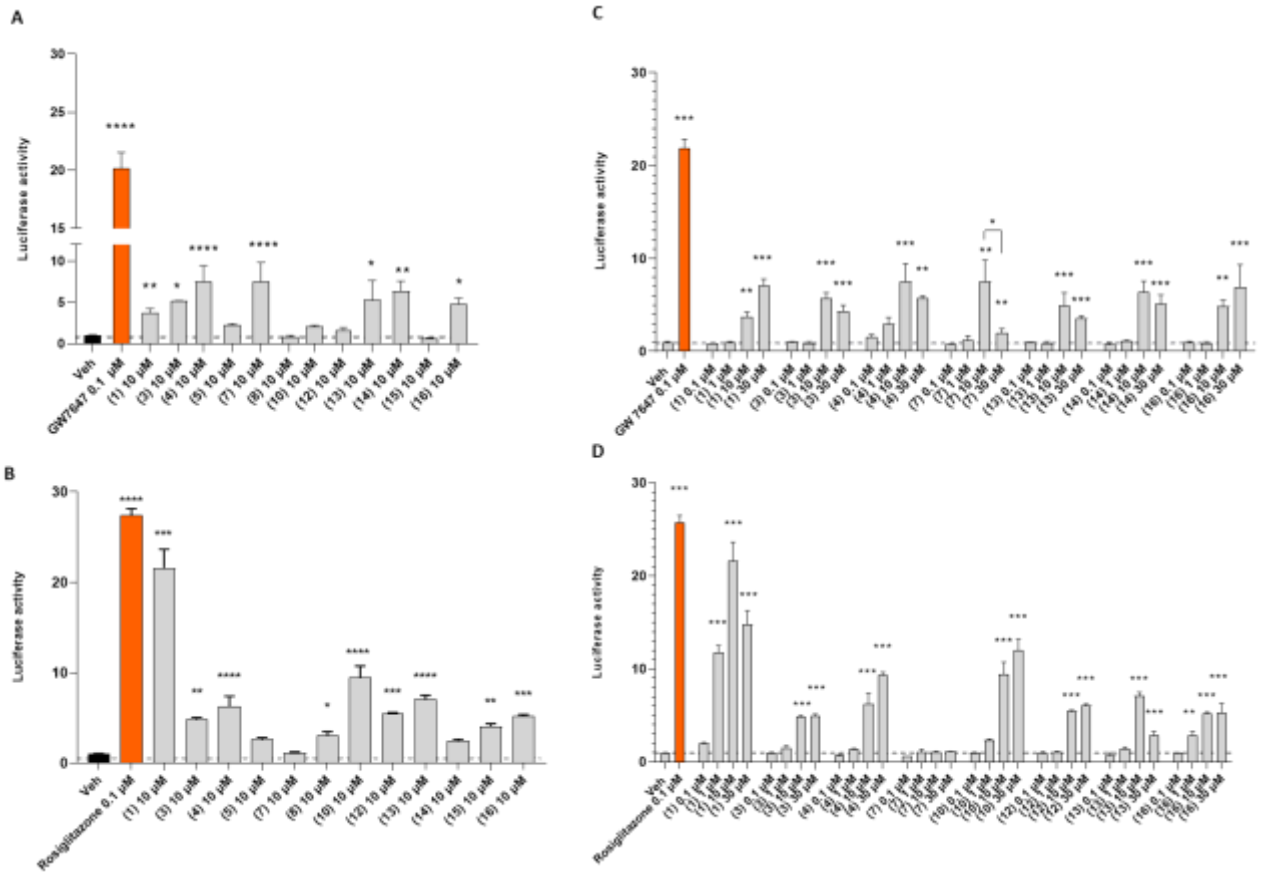

Figure 5: Effect of natural amorfrutin derivates on PPARα and/or PPARγ activity in COS-7 cells. Relative Luciferase Units in response to 10 µM of test compounds on PPARα **(A)** and PPARγ **(B).** Concentration-response effect of test compounds on PPARα **(C)** and PPARγ **(D).** The activity of the vehicle control was set at 1 and the relative luciferase activities obtained for each compound and dose tested are presented as fold induction to the vehicle control. Each bar is the mean ± S.E.M. from 3-4 independent biological samples. ****P ≤ 0.0001; ***P ≤ 0.0003; **P ≤ 0.003; *P ≤ 0.05 vs. the indicated experimental group calculated using ANOVA or unpaired Student's t-test using GraphPad Prism 7 software.

In silico study and structure-activity relationships. Insights into the PPARα/γ binding mode of the most active amorfrutins were obtained by a combined approach of molecular docking and molecular dynamics (MD) simulations. For each compound, the most relevant binding poses from docking, selected on the basis of binding energy, cluster

population and visual inspection, underwent 100ns of MD to assess their stability. If rearrangements occurred during MD, the stability of the new pose was evaluated for additional 50-100 ns. Only docking poses remaining stable for at least 60ns during MD were considered for structure-activity relationships (SARs) (Figure S2). The crystal structure of amorfrutin A (**1**) complexed to PPARγ has been reported;[7] conversely, no experimental data are available for its interaction with PPARα, where it is also active, albeit with lower potency than on PPARγ. Thus, its binding mode was investigated in silico and two alternative binding poses were found (pose 1A and 1B), characterized by a reversed orientation of the phenylethyl moiety (Figure 6).

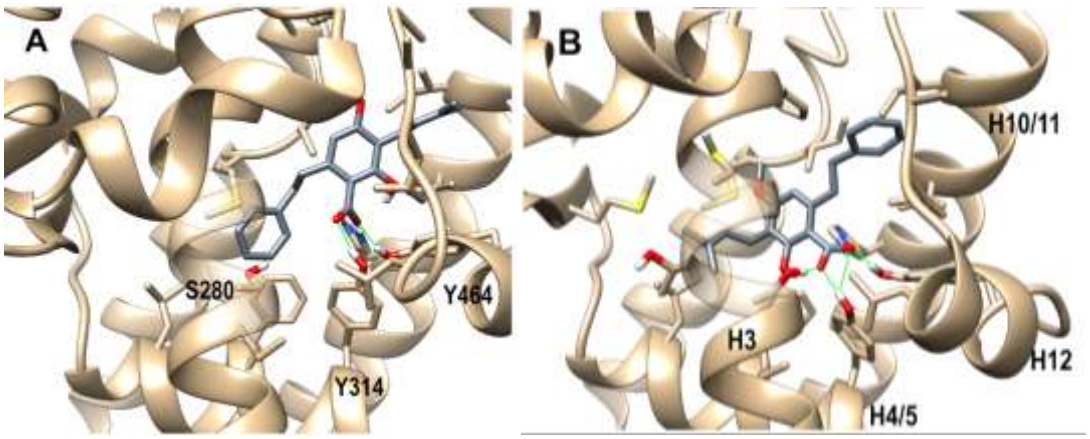

Figure 6. Representative MD frames of PPARα LBD (tan) in complex with amorfrutin A (**1,** slate gray). Poses A and B discussed in the text are shown in panel A and B, respectively. Ligand and protein sidechains within 4 Å from the ligand are shown in stick representation. Oxygen, nitrogen, and sulfur atoms are colored red, blue, and yellow, respectively. H-bonds are shown as green sticks.

In both poses, the carboxylate group forms a network of H-bonds involving Tyr314 (H4/5), His440 (H10/11) and Tyr464 (H12) sidechains, while in pose B an additional H-bond with Ser280 (H3) sidechain is observed. The network of H-bonds engaged by the ligand within the LBD is compatible with full agonism, but the pattern of interaction confines the ligand in a polar sub-pocket, with an overall limited occupancy of the LBD. Amorfrutin C (**10**) was the second most active PPARγ agonist with negligible activity on PPARα. Its stable binding modes at PPARγ are shown in Figure S3. In analogy to amorfrutin A (**1**) interaction,

the binding site encompasses helix H3, the β-sheet and the Ω-loop. Two main orientations are adopted by the phenethyl chain which points toward Phe264 on Ω-loop in orientation A, and to the opposite direction in orientation B. Orientation A optimizes either the π-π stacking, or the ionic interaction between Arg288 (H3) and the carboxylate group, while in orientation B, a cation-π interaction with Arg288 (H3) takes place. Amorfrutin C (**10**) differs from amorfrutin A (**1**) only for an additional isoprene group decorating the resorcinol ring. This additional substituent exerts a detrimental effect on the activity at both receptors. At PPARα, it induces steric hindrance preventing the binding at the hydrophilic sub-pocket which hosts instead amorfrutin A (**1**) (data not shown). At PPARγ, it increases both the entropic cost upon binding, due to the flexible additional pendant, and the number of suboptimal binding modes in terms of receptor activation.

The racemic amorfrutin J (**13**) behaves as a dual PPARα/γ agonist. The binding modes of the two enantiomers, hosted in the polar sub-pocket which comprises helix H12, are similar in the two receptor isoforms. In PPARα LBD, the carboxylate group forms a network of H-bonds with the side chains of Tyr314 (H4/5), His440 (H10/11), Ser 280 (H3) and Tyr464 (H12). The hydroxyl group of the stereogenic carbon is involved in H-bond with Gln277 (H3) sidechain in the *R* enantiomer alone, as shown in Figure 7. In PPARγ LBD, the carboxylate group is involved in the same pattern of PPARα H-bonds, except for PPARα Tyr314, now replaced by His323 (H4/5). However, the ligand adopts a flipped orientation for PPARα, its pentyl chain now pointing toward helix H10/11. This reversed orientation is probably due to the occurrence of Phe363 (H7) in place of PPARα Ile354, which changes the accessible surface size/shape of this hydrophobic cleft.

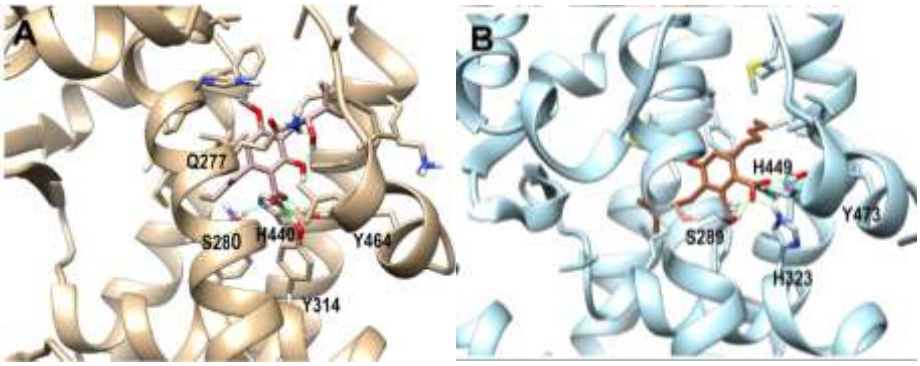

Figure 7. Panel A: representative MD frame of PPARα LBD (tan) in complex with the *R* enantiomer of amorfrutin J (**13,** rose brown). Panel B: representative MD frame of PPARγ LBD (light blue) in complex with the *S* enantiomer of amorfrutin J (**13,** sienna). Ligand and protein sidechains within 4 Å from the ligand are shown in stick representation. Oxygen, nitrogen, and sulfur atoms are colored red, blue, and yellow, respectively. H-bonds are shown as green sticks.

The situation of amorfrutin 3 (**3**), again a dual PPARα/γ agonist, is quite similar to that of **13**, since the two compounds differ only for the side chain (phenethyl in the former and pentyl in the latter). The binding poses of the two enantiomers of **3** at PPARα are similar to those of **13**. Conversely, at PPARγ the preferred binding site is located between the β-sheet and helix H3, recapping the binding mode of the other amorfrutins with the same pendant. The binding poses of both enantiomers are stabilized by π-π stacking between the phenyl group and Phe264 on Ω-loop and by H-bonds engaged by the carboxylate group with Ser342 sidechain on the β-sheet. The *S* enantiomer forms an additional H-bond involving the hydroxyl group of the stereogenic center with the backbone atoms of Leu340 and Ser342 (see Figure S4).

The racemic amorfrutin E (**4**) shows a dual agonist profile. Both enantiomers can adopt two binding poses within the LBD of PPARα, depending on the orientation of the phenyl pendant, which can alternatively point toward the helix H10/11 (up pose), or the β-sheet (down pose). In the up pose, the carboxylate group of S enantiomer is involved in H-bonds with His440 (H10/11) and Tyr314 (H4/5), Ser280 (H3) and Tyr464 (H12), and the hydroperoxide group is involved in H-bond with Ser280 (H3) sidechain. In this pose, the (*R*)

enantiomer moves away from helix H12, due to the formation of a H-bond between the peroxide group and Cys276 (H3) (data not shown). In the down pose, both enantiomers engage the same pattern of H-bonds with His440 (H10/11) and Tyr314 (H4/5), Ser280 (H3) and Tyr464 (H12) but the peroxide group is now involved in H-bond with Gln277 (H3) sidechain (Figure 8).

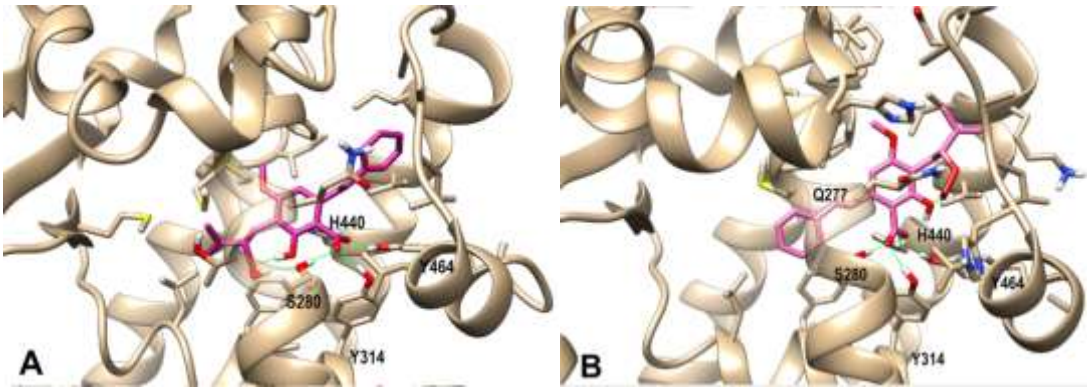

Figure 8. Representative MD frames for the up pose (panel A) and down pose (panel B) of PPARα LBD (tan) in complex with the *S* (magenta, panel A) and *R* (pink, panel B) enantiomers of amorfrutin E (**4**). Ligand and protein sidechains within 4 Å from the ligand are shown in stick representation. Oxygen, nitrogen, and sulfur atoms are colored red, blue, and yellow, respectively. H-bonds are shown as green sticks.

In the LBD of PPARγ, both enantiomers are hosted in the cleft between the β-sheet and helix H3, where they form π-π stacking between their phenyl ring and Phe264 on Ω-loop. Alternative poses have been obtained for both enantiomers. The carboxylate group is involved in H-bonds with backbone atoms and/or Ser342 sidechain of the β-sheet and/or in H-bond/ionic interactions with Arg288 (H3). The peroxide group of the R enantiomer can alternatively form H-bonds with Arg288 (H3) or Cys285 (H3) sidechains, while that of the S enantiomer is H-bonded to either Ser342 sidechain and Ω-loop backbone atoms, or backbone atoms of helix H3 (Figure S5).

While devoid of PPARγ agonist activity, amorfrutin H (**7**) was, along with amorfrutin E (**4**), the most potent PPARα agonist. To rationalize this behavior, a computational study was undertaken at both receptor isoforms. At PPARα, amorfrutin H (**7**) binds in the polar sub-

pocket of the LBD encompassing helix H12, where it engages a network of stable H-bonds between its carboxylate group and His440 (H10/11), Ser280 (H3) and Tyr314 (H4/5) sidechains, while its methoxy group forms H-bond with Q277 (H3). The phenyl group is hosted in a hydrophobic cleft formed by Phe273 (H3), Leu344 (H6), Ile354 and Met355 (H7). The representative MD frame for this complex is shown in Figure 9A. A stable complex was also obtained for PPARγ (Fig. 9B), where amorfrutin H binds near the β-sheet and is involved in both H-bonds with Ser342 (β-sheet), His266 (Ω-loop), and π-π stacking with Phe264 and His266 (Ω-loop). This stable binding mode prompted us to evaluate by luciferase assay a possible activity as a PPARγ antagonist for this compound. As shown in figure 9C, amorfrutin H is indeed able to significantly antagonize the effect of rosiglitazone.

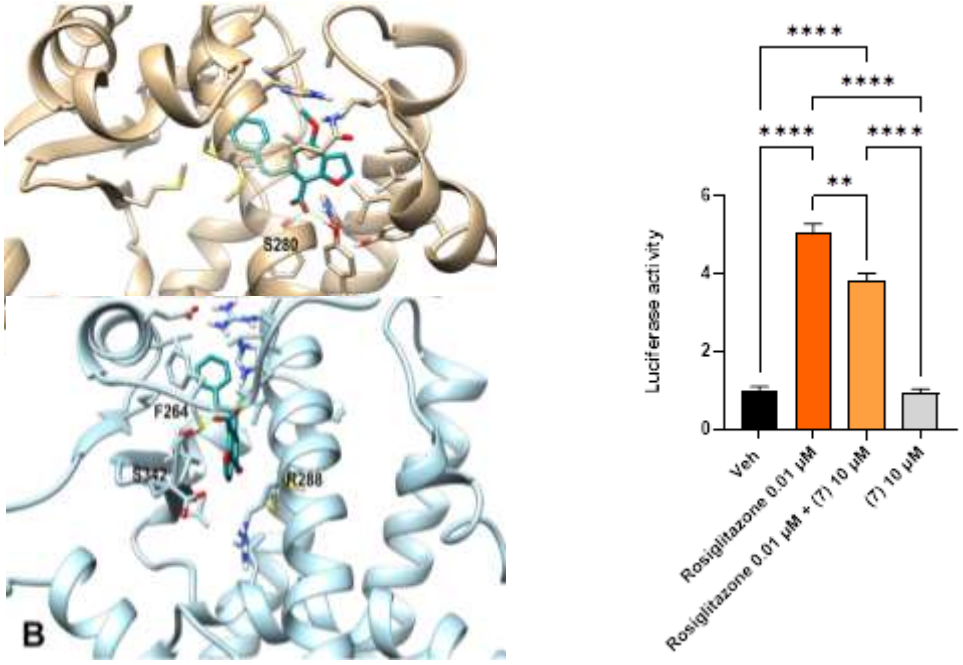

Figure 9. Panel A: representative MD frames of PPARα (tan, panel A) and PPARγ LBD (light blue, panel B) in complex with amorfrutin H (**7**) (dark cyan). Ligand and protein sidechains within 4 Å from the ligand are shown in stick representation. Oxygen, nitrogen, and sulfur atoms are colored red, blue, and yellow, respectively. H-bonds are shown as green sticks. Panel C: Effect of amorfrutin H (**7**) on PPARγ activity induced by rosiglitazone 0.01 µM**.** The activity of the vehicle control was set at 1 and the relative luciferase activities obtained for each compound and dose tested are presented as fold induction to the vehicle control. Each bar is the mean ± S.E.M. from 3-4 independent biological samples. ****P ≤ 0.0001; **P ≤ 0.003 vs. the indicated experimental group calculated using ANOVA using GraphPad Prism 7 software.

The racemic amorfrutin K (**14**) showed a stronger activity toward PPARα, being a weak PPARγ agonist. At PPARα, the enantiomers adopt a similar binding pose and engage H-bonds between carboxylate group and residues lying in the polar cleft encompassing helix H12, such as Ser280 (H3) and Tyr314 (H4/5), His440 (H10/11), and Tyr464 (H12), but only the *R* enantiomer forms an additional H-bond between its hydroxyl group and Ser 280 (H3), as shown in Figure 10. Intriguingly, **14** shares a similar structure of the isoprenoid region compared to amorfrutin H (**7**), thus suggesting a detrimental effect of this moiety on PPARγ agonism.

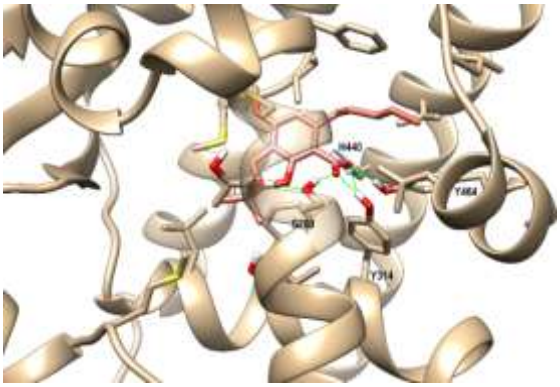

Figure 10. Representative MD frame of PPARα (tan) LBD in complex with the *R* enantiomer of amorfrutin K (**14**, coral). Ligand and protein sidechains within 4 Å from the ligand are shown in stick representation. Oxygen, nitrogen, and sulfur atoms are colored red, blue, and yellow, respectively. H-bonds are shown as green sticks.

The binding mode of amorfrutin M (**16**) (see Figure 11A) is similar at both receptors, with the two isoprene arms adopting a horseshoe arrangement around helix H3, and the resorcinol moiety engaged in H-bond with Ser280(PPARα)/289 (PPARγ), accounting for its activity as dual PPARα/γ agonist. The binding mode of compound **12**, a selective PPARγ agonist, is shown in Figure 11B. As for compound **16**, the resorcinol moiety is involved in a H-bond with Ser289 (H3). However, in this case, the lack of one isoprene substituent allows π-π stacking between the resorcinol moiety and Phe363 (H7). This stabilizing interaction is

missing in PPARα, where a residue of isoleucine occurs in place of Phe363 (H7), and this could explain the lack of activity at this receptor.

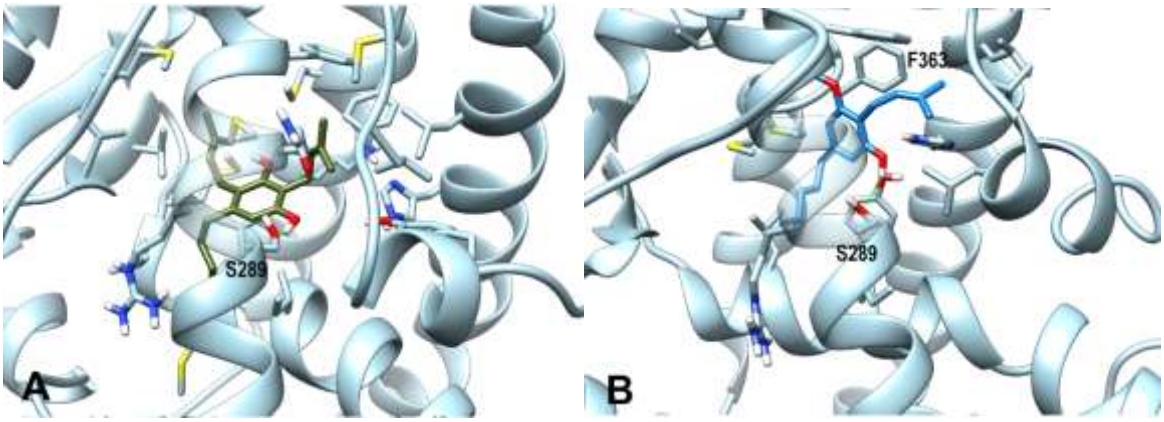

Figure 11. Representative MD frames of PPARγ (light blue) LBD in complex with compound **16** (dark green, panel A) and **12** (dodger blue, panel B). Ligand and protein sidechains within 4 Å from the ligand are shown in stick representation. Oxygen, nitrogen, and sulfur atoms are colored red, blue, and yellow, respectively. H-bonds are shown as green sticks.

CONCLUSIONS

The biosynthetic profligacy of *G. foetida* provided a set of amorfrutins which included many compounds with an oxygenated or truncated isoprenyl moiety, an element of the biological space of amorfrutins still substantially unexplored. In some cases, oxidation was associated with the formation of stereogenic centers and all the chiral compounds were obtained in racemic form. This could be due either to the poor enantioselectivity of the oxidase biosynthetic steps or to a non-enzymatic auto-oxidation of the prenyl group. The structural diversity of the amorfrutins available by isolation was complemented by the synthesis of analogues edited on the aralkyl moiety, another unexplored area of the biological space of these compounds. All compounds were assayed for agonist activity on PPARα and PPARγ nuclear receptors. Amorfrutin A (**1**) proved to be the most potent agonist of PPARγ, followed by amorfrutin C (**10**), while the single compound including a benzofuran moiety, amorfrutin H (**7**), selectively activated PPARα and significantly antagonized the effect of rosiglitazone on PPARγ. Amorfrutins E (**4**), 3 (**3**), and J (**13**) behaved as dual

agonists, and interestingly, regardless of the pentyl or phenethyl chains, they had practically the same 2'-oxygenated prenyl moiety. Computational studies contributed to shed light on the binding of amorfrutins to PPARα/γ receptors, rationalizing the strict structure-activity relationships which characterize this interaction. Finally, decarboxyamorfrutin A (**2**) was cytotoxic, and editing its phenethyl moiety to a styryl or a phenylethynyl group, regardless of the degree of *O*-methylation, retained this trait, suggesting an alternative biological scenario for these compounds.

MATERIALS AND METHODS

General Experimental Procedures. Optical rotations ($CHCl_3$ and MeOH) were measured at 589 nm on a P2000 (JASCO Europe s.r.l., Cremella, Italy) polarimeter. ^1H (600 and 700 MHz) and ^{13}C (150 and 175 MHz) NMR spectra were measured on a Bruker spectrometer. Chemical shifts are referenced to the residual solvent signal ($CDCl_3$: δ_H 7.26, δ_C 77.0; CD_3OD: δ_H 3.31, δ_C 49.3). Homonuclear ^1H connectivities were determined by COSY (COrrelation SpectroscopY) experiments. Throughspace ^1H connectivities were evidenced using a NOESY (Nuclear Overhauser Enhancement SpectroscopY) experiment with a mixing time of 300 ms. One-bond heteronuclear ^1H–^{13}C connectivities was determined by the HSQC (Heteronuclear Single Quantum Correlation) experiment; two- and three-bond ^1H–^{13}C connectivities by gradient-HMBC (Heteronuclear Multiple Bond Correlation) experiments optimized for a $^{2,3}J$ of 8 Hz. HR-ESIMS experiments were performed on LTQ-Orbitrap mass spectrometer equipped with an ESI interface and Excalibur data system. MPLC-DAD separations were performed on an Interchim® instrument, puriFlash XS 520 Plus (Sepachrom s.r.l., Milan, Italy), using Purezza®-Daily Silica Cartridge 50Å 25µ - size 25 (25 g) – Column Volume (CV) 30 mL. HPLC-RI separations were performed on Knauer instruments, using Knauer 1800 apparatus equipped with a refractive index detector using Luna 5 µm Silica (2) 100 Å 250 x 4.6 mm

column, or Kinetex 264 C18 100 Å 100 × 4.6 mm for reverse-phase chromatography, equipped with a Rheodyne injector. RP-HPLC-UV-vis separation was performed on an Agilent instrument, using 1260 Quat Pump VL system, equipped with a 1260 VWD VL UV–vis detector using a Luna 10 µm C18 100 Å 250 × 10 mm column and a Rheodyne injector. Thin-layer chromatography (TLC) was performed on plates coated with silica gel 60 F254 Merck, 0.25 mm. Chemicals and solvents were from Merck Life Science S.r.l. and were used without any further purification unless stated otherwise.

Plant material and extraction. *G. foetida* aerial parts were collected in Fernana (northwestern Tunisia) in July 2019. The taxonomic identification was carried out by Dr Ridha El Mokni, affiliated to the Department of Pharmaceutical Sciences "A", Laboratory of Botany Faculty of Pharmacy of Monastir, Tunisia, where voucher specimen (GF 121) has been deposited. The aerial parts (600 g) were dried in the shade at room temperature until constant weight and then comminuted to powder and extracted exhaustively by maceration in methanol/dichlomethane (1:1 v/v) for 3 days (2.5 × 3 L) to afford 40 g of a crude extract after removal of the solvent under vacuum. This extract was defatted by suspension in *n*-hexane, then suspended in water (300 mL) and partitioned sequentially against dichloromethane (3 × 400 mL) and n-butanol (3 × 400 mL) obtaining dichloromethane (11. 3 g) and butanol (20.3 g) extracts, respectively.

LC-MS/MS Analysis. The qualitative profile of *G. foetida* Desf. aerial parts was obtained by LC-MS analysis carried out using an LTQ-XL Ion Trap mass spectrometer (Thermo Fisher Scientific Spa, Rodano, Italy) equipped with an Ultimate 3000 HPLC (Agilent Technology, Cernusco sul Naviglio, Italy). Chromatografic separation was achieved on a Kinetex 2.6 µm polar C18 100 Å (100 × 3 mm) column (Phenomenex, Torrance, CA, USA). The LC-MS/MS experiment was carried out using a combination of A (0.1% formic acid in water, v/v) and B (0.1% formic acid in MeCN, v/v) as mobile phase; the gradient elution was optimized as follows: 50% B for 3 min, 50% to 95% B over 20 min, held 10 min before

returning in the initial conditions. The total run time, including the column wash and the equilibration, was 30 min, flow rate 0.5 mL/min, injection volume 5 µL. The MS and MSn spectra, in positive mode, were recorded in Data Dependent Acquisition mode inducing fragmentation of the most intense five peaks for each scan. Source conditions were: spray voltage: 3.5 kV (positive mode); capillary voltage: 25 V; source temperature: 320 ◦C; normalized collision energy: 25. The acquisition range was m/z 150–1500. Source conditions: spray voltage 3.5 kV (positive mode); capillary voltage 25 V; source temperature 320 °C; normalized collision energy 25%. The acquisition range was m/z 150−1500. Although the spectra were recorded in both the positive and the negative modes, only the data obtained in positive mode have been taken into account.

Isolation of pure compounds. The dichlomethane extract (11.3 g) was purified on MPLC-DAD on a Silica Cartridge 50Å 25µ - size 25 (25 g) – column volume (CV) 30 mL/min. The mobile phase was a mixture of A: hexane, B: ethyl acetate and C: methanol with the following gradient method: starting conditions: 90%A – 10%B for CV 0-5; 90%A – 10%B to 50%A – 50%B for CV 5-40; 50%A – 50%B for CV 40-45; 50%A – 50%B to 100%B for CV 45-50; 100%B for CV 50-52; 100%C for 53-55 CV; flow rate was 25.0 mL/min. The UV detection wavelength was set at 275 nm. This separation afforded 16 fractions that were further purified by HPLC. Fractions 3, 4, 5 and 7 were purified on HPLC-RI equipped with a Rheodyne injector, on a Luna 5 µm Silica (2) 100 Å 250 x 4.6 mm, flow rate 1.0 mL/min using different percentages of hexane and ethyl acetate (EtOAc) as mobile phase. Fraction 3 (68.4 mg) was separated by using hexane:EtOAc 95:5 as mobile phase, to afford decarboxyamorfrutin 2 (**12**) (t_R = 6.5 min, 18.4 mg) and amorfrutin M (**16**) (t_R = 9.0 min, 1.6 mg). Fraction 4 (67.2 mg) afforded decarboxyamorfrutin A (**2**) (t_R = 15.0 min, 4.7 mg), amorfrutin 2 (**11**) (t_R = 16.0 min, 8.6 mg) and decarboxydemethoxy amorfrutin C (**9**) (t_R = 24.8 min, 3.0 mg), while fraction 5 (64.3 mg), purified using hexane:EtOAc 9:1, led to the isolation of amorfrutin C (**10**) (t_R = 8.6 min, 2.0 mg) and amorfrutin A (**1**) (t_R = 9.5 min, 15.4

mg). Fraction 7 (50.3 mg) was separated using hexane:EtOAc 85:15 as eluent to yield amorfrutin H (**7**) (t_R = 19.7 min, 2.0 mg). Fraction 9 was purified using hexane:EtOAc 7:3 to afford amorfrutin J (**13**) (t_R = 4.2 min, 2.1 mg), amorfrutin E (**4**) (t_R = 3.8 min, 1.9 mg), amorfrutin L (**15**) (t_R = 8.6 min, 1.9 mg) and amorfrutin I (**8**) (t_R = 17.5 min, 2.0 mg). Fraction 11 was purified on RP-HPLC-RI using MeOH:H_2O 7:3 + 0.1% of formic acid on a Kinetex 264 C18 100 Å 100 × 4.6 mm, flow rate 1 mL/min, to achieve amorfrutin F (**5**) (t_R = 8.2 min, 2.4 mg), amorfrutin K (**14**) (t_R = 9.5 min, 1.9 mg) and amorfrutin 3 (**3**) (Rt = 14.9 min, 1.7 mg). Fraction 13 was purified on RP-HPLC-UV using an isocratic method H_2O + 0.1% of formic acid and acetonitrile 45:55, UV-detection was settled at λ = 276 nm, flow rate 3.0 mL/min, collecting amorfrutin G (**6**) (t_R = 9.5 min, 0.7 mg).

*Amorfrutin E (**4**).* Colorless amorphous solid, $[\alpha]_D$ 0 (c 0.21, $CHCl_3$); ^{1}H NMR ($CDCl_3$, 600 MHz): 7.28 (2H, overlapped, H-5', H-7'), 7.18 (1H, t, *J* = 7.1 Hz, H-6'), 7.17 (2H, d, *J* = 7.1 Hz, H-4', H-8'), 6.20 (1H, s, H-4), 4.99 (1H, s, H-4''a), 4.95 (1H, s, H-4''b), 4.44 (1H, dd, *J* = 8.8, 4.1 Hz, H-2''), 3.78 (3H, s, OMe), 3.26 (2H, m, H-1'), 3.14 (1H, dd, *J* = 8.8, 5.1 Hz, H-1a''), 3.02 (1H, dd, *J* = 13.7, 4.1 Hz, H-1''b), 2.91 (2H, t, *J* = 7.8 Hz, H-2'), 1.89 (3H, s, H-5''); ^{13}C NMR ($CDCl_3$, 150 MHz): 173.4 (COOH), 162.0 (C-3), 146.7 (C-5), 144.7 (C-1), 144.6 (C-3''), 142.1 (C-3'), 128.5 (C-4', C-8'), 128.3 (C-5', C-7'), 126.0 (C-6'), 112.6 (C-4''), 111.5 (C-2), 106.5 (C-4), 103.8 (C-6), 86.5 (C-2''), 55.5 (OMe), 39.6 (C-1'), 37.6 (C-2'), 24.0 (C-1''), 19.5 (C-5'')**;** ESIMS *m/z* 395 $[M + Na]^+$; HR-ESIMS found 395.1469 ($C_{21}H_{24}O_6Na$ requires 395.1471).

*Amorfrutin F (**5**).* Colorless amorphous solid, $[\alpha]_D$ 0 (c 0.24, $CHCl_3$); ^{1}H NMR ($CDCl_3$, 600 MHz): 7.26 (2H, overlapped, H-4', H-8'), 7.25 (2H, overlapped, H-5', H-7'), 7.17 (1H, t, *J* 6.8 Hz, H-6'), 6.22 (1H, s, H-4), 4.85 (1H, t, *J* 8.6 Hz, H-2''), 3.78 (3H, s, OMe), 3.31 (2H, m, H-1'), 3.13 (2H, d, *J* 8.6 Hz H-1''), 2.88 (2H, t, *J* 8.0 Hz, H-2'), 1.39 (1H, s, H-5''), 1.25 (1H, s, H-4''); ^{13}C NMR ($CDCl_3$, 150 MHz): 172.9 (COOH), 160.1 (C-1), 158.5 (C-3), 148.5 (C-5), 142.0 (C-3'), 128.4 (C-5', C-7'), 126.0 (C-4', C-8'), 125.7 (C-6'), 112.1 (C-2), 108.1 (C-4),

104.5 (C-6), 92.3 (C-2''), 71.8 (C-3''), 55.5 (OMe), 37.9 (C-2'), 37.8 (C-1'), 27.5 (C-1''), 26.2 (C-5''), 24.2 (C-4''). ESI *m/z* 357 $[M + H]^+$; HR-ESIMS found *m/z* 357.1699 ($C_{21}H_{25}O_5$ requires 357.1702).

*Amorfrutin G (**6**).* Colorless amorphous solid, $[\alpha]_D$ 0 (c 0.10, $CHCl_3$); ^1H NMR ($CDCl_3$, 600 MHz): 7.26 (2H, overlapped, H-5', H-7'), 7.21 (2H, overlapped, H-4', H-8'), 7.19 (1H, overlapped, H-6'), 6.27 (1H, s, H-4), 5.10 (1H, d, *J* = 3.0 Hz, H-1''), 4.59 (1H, d, *J* = 3.0 Hz, H-2''), 3.82 (3H, s, OMe), 3.44 (3H, s, OMe''), 3.39 (2H, m, H-1'), 2.90 (2H, m, H-2'), 1.32 (3H, s, H-5''), 1.30 (3H, s, H-4''); ^{13}C NMR ($CDCl_3$, 150 MHz): 173.3 (COOH),162.3 (C-1), 159.7 (C-3), 145.1 (C-5), 141.3 (C-3'), 128.8 (C-5', C-7'), 128.2 (C-4', C-8'), 125.8 (C-6'), 111.8 (C-2), 108.3 (C-4), 104.7 (C-6), 96.3 (C-2''), 79.0 (C-1''), 71.2 (C-3''), 56.4 (OMe-1''), 55.7 (OMe-3), 37.9 (C-1'), 37.6 (C-2'), 25.5 (C-5''), 25.2 (C-4''); ESIMS *m/z* 409 $[M + Na]^+$; HR-ESIMS found *m/z* 409.1622 ($C_{22}H_{26}O_6Na$ requires 409.1627).

*Amorfrutin H (**7**).* Colorless amorphous solid; ^1H NMR ($CDCl_3$, 600 MHz): 7.62 (1H, s, H-2''), 7.27 (2H, t, *J* = 7.4 Hz, H-5', H-7'), 7.22 (2H, d, *J* = 7.4 Hz, H-4', H-8'), 7.19 (1H, t, *J* = 7.4 Hz, H-6'), 6.87 (1H, s, H-1''), 6.41 (1H, s, H-4), 3.88 (3H, s, OMe), 3.40 (2H, t, *J* = 7.8 Hz, H-1'), 2.97 (2H, t, *J* = 7.8 Hz, H-2'); ^{13}C NMR ($CDCl_3$, 150 MHz): 172.9 (COOH), 156.7 (C-1), 156.3 (C-3), 145.1 (C-5), 143.5 (C-2''), 141.8 (C-3'), 128.7 (C-4', C-8'), 128.3 (C-5', C-7'), 125.9 (C-6'), 116.7 (C-2), 107.8 (C-4), 106.2 (C-6), 104.2 (C-1''), 56.2 (OMe), 38.1 (C-2'), 37.2 (C-1'); ESIMS *m/z* 297 $[M + H]^+$; HR-ESIMS found 297.1126 ($C_{18}H_{17}O_4$ requires 297.1127).

*Amorfrutin I (**8**).* Colorless amorphous solid, $[\alpha]_D$ 0 (c 0.20, $CHCl_3$); ^1H NMR ($CDCl_3$, 600 MHz): 7.28 (2H, overlapped, H-4', H-8'), 7.28 (2H, overlapped, H-5', H-7'), 7.18 (1H, br s, H-6'), 6.29 (1H, s, H-4), 3.88 (1H, d, *J* = 5.3 Hz, H-2''), 3.78 (3H, s, OMe), 3.29 (2H, t, *J* = 7.3 Hz, H-1'), 2.92 (1H, overlapped, H-1a''), 2.91 (2H, overlapped, H-2'), 2.67 (1H, dd, *J* = 17.4, 5.3 Hz, H-1''b), 1.46 (1H, s, H-5''), 1.44 (1H, s, H-4''); ^{13}C NMR ($CDCl_3$, 150 MHz): 175.0 (COOH), 160.0 (C-3), 152.5 (C-1), 147.7 (C-5), 142.1 (C-3'), 128.8 (C-4', C-8'), 128.8

(C-5', C-7'), 125.9 (C-6'), 110.5 (C-6), 107.2 (C-4), 106.5 (C-2), 80.0 (C-3''), 68.6 (C-2''), 55.9 (OMe), 38.7 (C-1'), 37.5 (C-2'), 26.3 (C-1''), 24.9 (C-4''), 21.8 (C-5''); ESIMS *m/z* 357 $[M + H]^+$; HR-ESIMS found 357.1695 ($C_{21}H_{25}O_5$ requires 357.1702).

*Decarboxydemethoxy amorfrutin C (**9**):* Colorless amorphous solid; ^{1}H NMR ($CDCl_3$, 600 MHz): 7.29 (2H, t, *J* = 7.1 Hz, H-5', H-7'), 7.20 (1H, overlapped, H-6'), 7.19 (2H, overlapped, H-4', H-8'), 6.30 (1H, s, H-6), 5.26 (1H, t, *J* = 6.9 Hz, H-2'''), 5.10 (1H, t, *J* = 6.4 Hz, H-2''), 3.40 (2H, d, *J* = 6.9 Hz, H-1'''), 3.30 (2H, d, *J* = 6.4 Hz, H-1''), 2.82 (4H, overlapped, H-1', H-2'), 1.82 (3H, s, H-4'''), 1.80 (3H, s, H-4''), 1.75 (3H, s, H-5'''), 1.73 (3H, s, H-5''); ^{13}C NMR ($CDCl_3$, 150 MHz): 153.9 (C-3), 152.9 (C-1), 142.0 (C-3'), 138.9 (C-5), 134.8 (C-3'''), 134.3 (C-3''), 128.5 (C-5', C-7'), 128.4 (C-4', C-8'), 126.1 (C-6'), 122.9 (C-2''), 122.4 (C-2'''), 117.4 (C-2), 111.9 (C-4), 109.3 (C-6), 37.7 (C-2'), 35.6 (C-1'), 26.1 (C-5'''), 26.1 (C-5''), 25.6 (C-1''), 25.6 (C-1'''), 18.4 (C-4''), 18.4 (C-4'''); ESIMS *m/z* 351 $[M + H]^+$; HR-ESIMS *m/z* found 351.2312 ($C_{24}H_{31}O_2$ requires 351.2324).

*Amorfrutin J (**13**):* Colorless amorphous solid, $[\alpha]_D$ 0 (c 0.19, $CHCl_3$); ^{1}H NMR ($CDCl_3$, 600 MHz): 6.35 (1H, s, H-4), 4.99 (1H, s, H-4''a), 4.83 (1H, s, H-4''b), 4.26 (1H,dd, *J* = 9.0, 3.1 Hz, H-2''), 3.88 (3H, s, OMe), 3.03 (1H, dd, *J* = 13.9, 3.2 Hz, H-1''a), 2.92 (2H, overlapped, H-1'), 2.91 (1H, overlapped, H-1''b), 1.85 (3H, s, H-5''), 1.58 (2H, overlapped, H-2'), 1.35 (2H, overlapped, H-3'), 1.34 (2H, overlapped, H-4'), 0.90 (3H, t, *J* 6.7 Hz, H-5'); ^{13}C NMR ($CDCl_3$, 150 MHz), 173.8 (COOH), 162.4 (C-3), 148.3 (C-5), 148.0 (C-1), 147.7 (C-3''), 112.2 (C-2), 110.0 (C-4''), 106.7 (C-4), 104.0 (C-6), 76.0 (C-2''), 55.8 (OMe), 37.2 (C-1'), 32.1 (C-3'), 31.7 (C-2'), 29.6 (C-1''), 22.5 (C-4'), 18.1 (C-5''), 14.1 (C-5'); ESIMS *m/z* 345 $[M + Na]^+$; HR-ESIMS found 345.1664 ($C_{18}H_{26}O_5Na$ requires 345.1678).

*Amorfrutin K (**14**):* Colorless amorphous solid, $[\alpha]_D$ 0 (c 0.12, $CHCl_3$); ^{1}H NMR ($CDCl_3$, 700 MHz): 6.36 (1H, s, H-4), 4.84 (1H, t, *J* = 8.8 Hz, H-2''), 3.87 (3H, s, OMe), 3.12 (2H, d, *J* = 8.8 Hz, H-1''), 3.02 (2H, m, H-1'), 1.57 (2H, m, H-2'), 1.37 (3H, s, H-5''), 1.35 (2H, overlapped, H-3'), 1.32 (2H, overlapped, H-4'), 1.24 (3H, s, H-4''), 0.89 (3H, t, *J* = 7.0 Hz, H-

5'); ^{13}C NMR ($CDCl_3$, 175 MHz): 173.1 (COOH), 160.3 (C-1), 158.7 (C-3), 111.6 (C-2), 149.5 (C-5), 107.5 (C-4), 104.9 (C-6), 92.0 (C-2''), 71.8 (C-3''), 55.5 (OMe), 35.3 (C-1'), 32.0 (C-3'), 31.6 (C-2'), 27.4 (C-1''), 26.0 (C-5''), 24.0 (C-4''), 22.4 (C-4'), 14.1 (C-5'); ESI m/z 323 $[M + H]^+$; HR-ESIMS found 323.1852 ($C_{18}H_{27}O_5$ requires 323.1858).

*Amorfrutin L (**15**):* Colorless amorphous solid, $[\alpha]_D$ 0 (c 0.12, $CHCl_3$); ^{1}H NMR ($CDCl_3$, 600 MHz): 6.41 (1H, s, H-4), 3.86 (1H, overlapped, H-2''), 3.86 (3H, s, OMe), 2.98 (2H, m, H-1'), 2.91 (1H, dd, *J* = 17.7, 5.1 Hz, H-1''a), 2.67 (1H, dd, *J* = 17.4, 5.6 Hz H-1''b), 1.60 (2H, overlapped, H-2'), 1.37 (2H, overlapped, H-3'), 1.37 (3H, s, H-5''), 1.36 (2H, overlapped, H-4'), 1.35 (3H, s, H-4''), 0.89 (3H, t, *J* = 7.0 Hz, H-5'); ^{13}C NMR ($CDCl_3$, 150 MHz), 174.9 (COOH), 159.9 (C-3), 152.4 (C-1), 148.8 (C-5), 113.2 (C-2), 110.8 (C-6), 106.4 (C-4), 78.5 (C-3''), 68.5 (C-2'') 55.7 (OMe), 36.0 (C-1'), 32.2 (C-3'), 29.5 (C-2'), 26.2 (C-1''), 24.6 (C-4''), 22.3 (C-4'), 21.5 (C-5''), 14.0 (C-5'); ESIMS *m/z* 345 $[M + Na]^+$; HR-ESIMS found 345.1684 ($C_{18}H_{26}O_5Na$ requires 345.1678).

*Amorfrutin M (**16**):* Colorless amorphous solid, $[\alpha]_D$ 0 (c 0.16, $CHCl_3$); ^{1}H NMR ($CDCl_3$, 600 MHz): 6.26 (1H, s, H-6), 5.25 (1H, tt, *J* = 7.0, 1.3 Hz, H-2''), 5.13 (1H, tt, *J* 6.7, 1.3 Hz, H-2'''); 3.38 (2H, d, *J* = 7.0 Hz, H-1''), 3.28 (2H, d, *J* = 6.7 Hz, H-1'''), 2.50 (2H, t, *J* = 7.7 Hz, H-1'), 1.81 (6H, s, H-4'', H-4'''), 1.74 (6H, s, H-5'', H-5'''), 1.51 (2H, m, H-2'), 1.33 (2H, overlapped, H-3'), 1.33 (2H, overlapped, H-4'), 0.89 (3H, t, *J* 7.2 Hz, H-5'); ^{13}C NMR ($CDCl_3$, 150 MHz) 153.7 (C-3), 152.8 (C-1), 140.0 (C-5), 134.9 (C-3''), 133.9 (C-3'''), 122.9 (C-2'''), 122.6 (C-2''), 117.1 (C-4), 111.5 (C-2), 108.8 (C-6), 33.5 (C-1'), 31.9 (C-3'), 31.1 (C-2'), 25.9 (C-5''), 25.9 (C-5'''), 25.4 (C-1'''), 22.6 (C-4'), 22.6 (C-1''), 17.8 (C4'''), 17.4 (C-4''), 14.0 (C-5'); ESIMS *m/z* 317 $[M + H]^+$; HRESIMS *m/z* found 317.2469 ($C_{21}H_{33}O_2$ requires 317.2481).

Synthesis of amorfrutin-type derivatives.

Diazotization-iodination of 3,5-dimethoxyaniline: To a cooled (0°C) stirred solution of 3,5-dimethoxyaniline (**22**, 5 g, 32.64 mmol) in water (50 mL), sulfuric acid (5 mL) was slowly added, then a solution of sodium nitrite (3.38 g, 48.96 mmol, 1.5 molar equiv.) in water (20

mL) was added dropwise. After 15 minutes, a solution of potassium iodide (16.26 g, 97.92 mmol, 3 molar equiv.) in water (20 mL) and diethyl ether (50 mL) were sequencially added. The reaction was stirred vigorously at 0°C for 3 hours, then quenched with a satured solution of Na_2SO_3 and diluited with diethyl ether. The organic phase was washed with brine, dried, and evaporated. The crude product was purified by GCC (PE/EtOAc 9:1 as eluant) to afford **23a** (6 g, 70%) as a white solid. ^{1}H NMR (300 MHz, $CDCl_3$): δ 6.76 (d, *J* = 2.2 Hz, 3H), 6.39 (t, *J* = 2.2 Hz, 1H), 3.75 (s, 6H).

*Mono and bis -demethylation and MOM protection of **23a**:* To a cooled (0°C) stirred solution of **23a** (2.5 g, 9.47 mmol) in dry dichloromethane (40 mL) under nitrogen atmosphere, boron tribromide (1M solution in DCM, 18.93 mL, 18.93 mmol, 2 molar equiv) was added dropwise. The reaction was stirred at 0 °C for 3 hours, then quenched with a satured solution of $NaHCO_3$ and diluition with DCM. The organic phase was washed with brine, dried, and evaporated. The crude product was then dissolved in dichloromethane, and N,N-diisopropylethylamine (4.92 mL, 28.41 mmol, 3 molar equiv.) and chloromethyl methyl ether (1.08 mL, 14.20 mmol, 1.5 molar equiv.) were sequencially added. The mixture was stirred at room temperature for 12 hours, then quenched by the addition of 2*N* H_2SO_4 and diluition with DCM. The organic phase was washed with brine, dried, and evaporated. The crude was purified by GCC (PE/EtOAc 8:2 as eluant) to afford **23b** (2.35 g, 92% over two steps) as orange oil. ^{1}H NMR (300 MHz, $CDCl_3$) δ 7.07 – 6.95 (m, 1H), 6.95 – 6.82 (m, 1H), 6.55 (t, *J* = 2.2 Hz, 1H), 5.12 (s, 2H), 3.76 (s, 3H), 3.46 (s, 3H). Repeating the same procedure with 4 molar equiv of boron tribromide (1M solution in DCM, 37.86 mL, 37.86 mmol), 6 molar equiv. of N,N-diisopropylethylamine (9.84 mL, 56.82 mmol), and 3 molaar equiv. of chloromethyl methyl ether (2.16 mL, 28.40 mmol), **23c** (orange oil, 1.47 g, 48% on two steps) was obtained. ^{1}H NMR (300 MHz, $CDCl_3$) δ 7.06 (d, *J* = 2.2 Hz, 2H), 6.68 (t, *J* = 2.2 Hz, 1H), 5.12 (s, 4H), 3.46 (s, 6H).

General procedure for Sonogashira coupling: A Schlenk tube was charged with **23a** (2 g,

7.57 mmol, 1 molar equiv), copper (I) iodide (15 mg, 0.08 mmol, 0.01 molar equiv.), bis-triphenylphosphine palladium (II) dichloride (53 mg, 0.08 mmol, 0.01 molar equiv.), triethylamine (2.11 mL, 15.14 mmol, 2 molar equiv), phenylacetylene (1.66mL, 15.14 mmol, 2 molar equiv.) and dry toluene (20 mL), then the mixture was degassed by three high vacuum/nitrogen cycles. The reaction was heated at 90 °C for 12 hours, then quenched by the addition of of 2*N* H_2SO_4 and diluition with EtOAc. The organic phase was washed with brine, dried, and evaporated. The crude was purified by GCC (PE/EtOAc 8:2 as eluant) to afford **24a** (1.93 g, 99%) as yellow oil. ^{1}H NMR (300 MHz, $CDCl_3$) δ 7.64 – 7.54 (m, 2H), 7.41-7.32 (m, 3H), 6.76 (d, *J* = 2.5 Hz, 2H), 6.51 (t, *J* = 2.2 Hz, 1H), 3.80 (s, 6H). 1,3-bis(methoxymethoxy)-5-(phenylethynyl)benzene (dark brown oil, 84%, **24b**) was obtained using **23c** as starting material. ^{1}H NMR (300 MHz, $CDCl_3$) δ 7.63–7.46 (m, 2H), 7.40–7.27 (m, 3H), 6.92 (d, *J* = 2.6 Hz, 2H), 6.74 (t, *J* = 2.3 Hz, 1H), 5.18 (s, 4H), 3.50 (s, 6H).

General procedure for Heck coupling: A Schlenk tube was charged with **23a** (350 mg, 1.33 mmol, 1 molar equiv), tetrabutylammonium bromide (1.53 g, 1.99 mmol, 1.5 molar equiv.), styrene (273 μL, 1.99 mmol, 1.5 molar equiv.), sodium acetate (176 mg, 2.15 mmol, 1.6 molar equiv), palladium acetate (16 mg, 0.07 mmol, 0.05 molar equiv.) and dry DMF (20 mL), then the mixture was degassed by 3 high vacuum/nitrogen cycles. The reaction was heated at 80 °C for 12 hours, then quenched by the addition of brine and diluition with Et_2O. The organic phase was washed dried and evaporated. The crude was purified by GCC (PE/EtOAc 9.1 as eluant) to afford **25a** (250 mg, 70%) as yellow oil. ^{1}H NMR (300 MHz, $CDCl_3$) δ 7.64–7.50 (m, 1H), 7.44–7.35 (m, 1H), 7.30 (d, *J* = 7.4 Hz, 0H), 7.10 (d, *J* = 5.0 Hz, 1H), 6.71 (d, *J* = 2.2 Hz, 1H), 6.44 (t, *J* = 2.2 Hz, 0H), 3.85 (s, 6H). 1-methoxy-3-(methoxymethoxy)-5-styrylbenzene (brown oil, 82%, **25b**) was obtained using **23b** as starting material. ^{1}H NMR (300 MHz, $CDCl_3$) δ 7.53 (d, *J* = 7.6 Hz, 2H), 7.38 (t, *J* = 7.6 Hz, 2H), 7.30 (d, *J* = 7.5 Hz, 1H), 7.10 (d, *J* = 7.4 Hz, 2H), 6.87 (m, 1H), 6.77 (m, 1H), 6.59 (m, 1H), 5.23 (s, 2H), 3.85 (s, 3H), 3.53 (s, 3H).

*Hydrogenation of **24b**:* Palladium on activated charcoal (10% Pd Basis, 286 mg, 0.27 mmol, 0.1 molar equiv.) was added to a solution of **24b** (800 mg, 2.68 mmol, 1 molar equiv.) in methanol (2 mL). The reaction was vigorously stirred under hydrogen atmosphere for 12 hours, until complete diseapparance of starting material (verified by ^{1}H NMR). The mixture was then filtered over a celite pad and the solvent evaporated. The crude resulted pure without any further purification, affording **26** (686 mg, 77%) as dark yellow oil. ^{1}H NMR (300 MHz, $CDCl_3$) δ 7.46–7.14 (m, 5H), 6.67–6.22 (m, 3H), 5.13 (s, 4H), 3.47 (s, 6H), 3.11–2.74 (m, 4H).

General procedure for isoprenylation: Buthyl lithium (575 μL, 1.44 mmol, 1.7 molar equiv.) was added dropwise under nitrogen atmosphere to a cooled (0 °C) solution of **24a** in dry THF. The mixture was stirred at 0 °C for 1 hour, then 3,3-dimethylallyl bromide (147 μL, 1.27 mmol, 1.5 molar equiv.) was added. The reaction was heated at 75 °C for 2 hours, then cooled to room temperature, quenched by the addition of 2*N* H_2SO_4 and diluition with EtOAc. The organic phase was washed with brine, dried and evaporated. The crude was purified by GCC (PE/DCM 9:1 as eluant) to afford **21** (500 mg, 82%) as dark yellow oil. ^{1}H NMR (300 MHz, $CDCl_3$) δ 7.63–7.47 (m, 2H), 7.47–7.27 (m, 3H), 6.72 (s, 2H), 5.16 (t, *J* = 7.2 Hz, 1H) 3.84 (s, 6H), 3.34 (d, *J* = 7.3 Hz, 2H), 1.76 (s, 3H), 1.67 (s, 3H). Using **25a** as starting material, 1,3-dimethoxy-2-(3-methylbut-2-en-1-yl)-5-styrylbenzene (yellow oil, 16%, **19**) was obtained. ^{1}H NMR (300 MHz, $CDCl_3$) δ 7.52 (d, *J* = 8.2 Hz, 2H), 7.36 (t, *J* = 7.7 Hz, 3H), 7.07 (s, 2H), 6.71 (s, 1H), 5.20 (t, *J* = 7.2 Hz, 1H), 3.88 (s, 6H), 3.36 (d, *J* = 7.4 Hz, 2H), 1.78 (s, 3H), 1.67 (s, 3H). Using **25b** as starting material, 1-methoxy-3-(methoxymethoxy)-2-(3-methylbut-2-en-1-yl)-5-styrylbenzene (yellow oil, 65%, **28**) was obtained. ^{1}H NMR (300 MHz, $CDCl_3$) δ 7.49 (d, *J* = 9.1 Hz, 2H), 7.32 (t, *J* = 8.0 Hz, 2H), 7.22 (t, *J* = 8.2 Hz, 1H), 7.05 (s, 1H), 6.91 (s, 1H), 6.74 (s, 1H), 5.24 (m, 3H), 3.84 (s, 3H), 3.48 (s, 3H), 3.39 (d, *J* = 6.6 Hz, 2H), 1.79 (s, 3H), 1.67 (s, 3H).

Chemoselective hydrogenation of triple bond: Lindlar catalyst (4 mg, 0.033 mmol, 0.1 molar equiv.) was added to a solution of **16** (100 mg, 0.325 mmol, 1 molar equiv.) in methanol (1 mL). The mixture was vigorously stirred under hydrogen atmosphere for 12 hours, until complete diseapparance of starting material (verified by ^{1}H NMR). The mixture was then filtered over a celite pad and the solvent evaporated. The crude resulted pure without any further purification, affording **17** (90 mg, 89%) as a yellow oil. ^{1}H NMR (300 MHz, $CDCl_3$) δ 7.47–7.16 (m, 5H), 6.38 (s, 2H), 5.21 (t, *J* = 7.4 Hz, 1H), 3.80 (s, 6H), 3.33 (d, *J* = 7.3 Hz, 2H), 2.92 (m, 4H), 1.78 (s, 3H), 1.68 (s, 3H).

General procedure for MOM deprotection: To a stirred solution of **28** (348 mg, 1.04 mmol, 1 molar equiv.) in methanol (15 mL, 15 mL/mmol), *p*-toluensulfonic acid (395 mg, 0.57 mmol, 0.5 molar equiv.) was added. The reaction was stirred at 50 °C for 2 hours, then quenched by the addition of a satured solution of $NaHCO_3$ and diluition with EtOAc. The organic phase was washed with brine, dried and evaporated. The crude was purified by GCC (PE/DCM 85:15 as eluant) to afford **20** (140 mg, 42%) as dark yellow oil. ^{1}H NMR (300 MHz, $CDCl_3$) δ 7.58 (d, *J* = 7.1 Hz, 2H), 7.43 (t, *J* = 7.4 Hz, 2H), 7.38 – 7.30 (m, 1H), 7.11 (s, 2H), 6.74 (s, 2H), 5.94 (OH, bs, 1H), 5.40 (t, *J* = 7.0 Hz, 1H), 3.94 (s, 3H), 3.55 (d, *J* = 6.7 Hz, 2H), 1.93 (s, 3H), 1.84 (s, 3H). Using **27** as starting material, 2-(3-methylbut-2-en-1-yl)-5-phenethylbenzene-1,3-diol (yellow oil, 22%, **18**) was obtained. ^{1}H NMR (300 MHz, $CDCl_3$) δ 7.44 – 7.05 (m, 5H), 6.26 (s, 2H), 5.35 – 5.26 (t, *J* = 7.4 Hz, 2H), 3.38 (d, *J* = 6.6 Hz, 2H), 3.06 – 2.60 (m, 4H), 1.82 (s, 3H), 1.75 (s, 3H).

Computational methods. Ligands were built with UCSF Chimera 1.17[14] followed by initial energy minimization (EM) at the molecular mechanics level, using AM1-BC charges. The molecules were then fully optimized using the GAMESS program[15] at the Hartree–Fock level with the STO-3G basis set and subjected to HF/6-31G*/STO-3G single-point calculations to derive the partial atomic charges using the RESP procedure.[16] Docking studies were performed with AutoDock 4.2 and Autodock Vina by using PPARα and PPARγ

crystallographic structures (PDB id: 2P54 and 6LX4 for PPARα and 2F4B and 2YFE for PPARγ). Two X-ray structures have been used for each receptor isoform to cope with differences both in Ω-loop and residue sidechain conformations. Both proteins and ligands were processed with AutoDock Tools (ADT) package version 1.5.6rc1[17] to merge non-polar hydrogens and calculate Gasteiger charges. Grids for docking evaluation with a spacing of 0.375 Å and 60 x 60 x 70 points, centered on the ligand binding site, were generated using the program AutoGrid 4.2 included in Autodock 4.2 distribution, following the docking protocol already published.[18] The complexes, selected on the basis of binding energy and cluster population, were completed by addition of all hydrogen atoms, and they underwent energy minimization (EM) and then molecular dynamics (MD) simulations with Amber20 pmemd.cuda module,[19] using the 14SB version of the AMBER force field for the protein and gaff parameters[20] for the ligand. To perform MD simulations in solvent, the complexes were confined in TIP3P water periodic boxes exhibiting a minimum distance between solute atoms and box surfaces of 10 Å, using the tleap module of the AmberTools20 package. The systems were then neutralized by addition of counterions (Na^+) and subjected to 1000 steps of EM, with solute atoms harmonically restrained to their starting positions (K_r = 10 kcal·mol^{-1}·Å^{-1}). Then, 500 ps of restrained MD (K_r = 5 kcal·mol^{-1}·Å^{-1}) at constant pressure was run on each solvated complex, gradually heating the system to 300 K, followed by 500 ps of restrained MD (K_r = 5 kcal·mol^{-1}·Å^{-1}) at constant temperature (300 K) and pressure (1 atm) to adjust system density. Production MD simulations were carried out at constant temperature (300 K) and pressure (1 atm) for 100 ns, with a time step of 2 fs. Bonds involving hydrogens were constrained using the SHAKE algorithm. The cpptraj module of AmberTools20 and program UCSF Chimera 1.17 were used to perform MD analysis and to draw the figures, respectively.

Cell culture, transfection and luciferase assay. COS-7 cells (monkey kidney fibroblast-like cells) were grown in DMEM supplemented with 10% fetal bovine serum and

1% Pen/Strep under standard conditions. For transfection, cells were plated in 24-well dishes. The day after, at about 60-70% confluence, cells were transfected using Lipofectamine 2000 Reagent (Cat# 11668019; Life Technologies MI Italy) with a mix of three plasmids a) CMX-Gal4-hPPARα; b) TK-MH100x4-Luc containing the UAS enhancer and c) Renilla Luciferase (pRL, Promega, Cat. E2231) according to the manufacturer's instruction. Cells transfected with an equal amount of pcDNA3.1 (Cat# V79020; Life Technologies MI Italy) were used as the control condition. On day 3, cells were treated for 24h with test compounds. Rosiglitazone 0.01 μM (Cat# 5325; Tocris UK) and GW7647 (Cat# 1677; Tocris UK) were used as positive internal controls for PPARγ and PPARα. At the end of treatment, the luciferase reporter activity was detected using the Dual-Glo® Luciferase Assay kit (Promega, Cat# E2920) using a GloMax® Discover microplate reader device.[18]

MTT assay. COS-7 cells were plated in 24 multiwell plates 2 x 105 per well. On the next day, cells were treated with test compounds for 24 h. DSMO (<0.03%), used to dissolve all compounds, was used as the control. Cell viability was assessed by the MTT assay following published procedures.[18] Briefly, the ability of cells to reduce MTT to formazan salts is assumed as a vitality sign being dependent on functional mitochondrial integrity. After 3 hrs of incubation, formazan salts were dissolved in 3 volumes of 2-methyl-2-propanol and absorbance read at 620 nm using a GloMax® Discover microplate reader device.

Notes

The authors declare no competing financial interest.

ACKNOWLEDGEMENTS

This research was partly funded by MUR, research grant PRIN2017, Project WN73PL (Bioactivity-directed exploration of the phytocannabinoid chemical space) and by EU funding within the MUR PNRR Extended Partnership initiative on Emerging Infectious Diseases (Project no. PE00000007, INF-ACT).

REFERENCES

(1). Hanuš, L. O.; Meyer, S. M.; Muñoz, E.; Taglialatela-Scafati, O.; Appendino, G. *Nat. Prod. Rep.* **2016**, *33*, 1357-1392.

(2). Mitscher, L. A.; Park, Y. H.; Alshamma, A.; Hudson, P. B.; Haas, T. *Phytochemistry* **1981**, *20*, 781-785.

(3). Ghisalberti, E. L.; Jefferies, P. R.; MacAdam, D. *Phytochemistry* **1981**, *20*, 1959-1961.

(4). Pollastro, F.; De Petrocellis, L.; Schiano-Moriello, A.; Chianese, G.; Heyman, H.; Appendino, G.; Taglialatela-Scafati, O. *Fitoterapia* **2017**, *123,* 13-17.

(5). Weidner, C.; de Groot, J. C.; Prasad, A.; Freiwald, A.; Quedenau, C.; Kliem, M.; Witzke, A.; Kodelja, V.; Han, C. T.; Giegold, S.; Baumann, M.; Klebl, B.; Siems, K.; Müller-Kuhrt, L.; Schürmann, A.; Schüler, R.; Pfeiffer, A. F.; Schroeder, F. C.; Büssow, K.; Sauer, S. *Proc. Natl. Acad. Sci U S A.* **2012**, *109*, 7257-62.

(6). Manfredi, K. P.; Vallurupalli, V.; Demidova, M.; Kindscher, K.; Pannell, L. K. *Phytochemistry* **2001**, *58*, 153-7.

(7). de Groot, J. C.; Weidner, C.; Krausze, J.; Kawamoto, K.; Schroeder, F. C.; Sauer, S.; Bussow, K. *J. Med. Chem.* **2013**, *56*, 1535−1543.

(8). Choi, H. W.; Tian, M.; Manohar, M.; Harraz, M. M.; Park, S. W.; Schroeder, F. C.; Snyder, S. H.; Klessig, D. F. *PLoS One* **2015**, *10*, e0143447.

(9). Fuhr, L.; Rousseau, M.; Plauth, A.; Schroeder, F. C.; Sauer, S. *J. Nat. Prod.* **2015**, *78*, 1160-1164.

(10). Sauer, S. *ChemBioChem* **2014**, *15*, 1231–1238.

(11). Chen, C.; Wu, Y.; Du, L*. Pharm. Biol.* **2016**, *54*, 488-493.

(12). Weidner, C.; Rousseau, M.; Micikas, R. J.; Fischer, C.; Plauth, A.; Wowro, S. J.; Siems, K.; Hetterling, G.; Kliem, M.; Schroeder, F. C.; Sauer, S. *J. Nat. Prod.* **2016**, *79*, 2-12.

(13). Sauer, S.; Weidner, C.; Kliem, M.; Schroeder, F. C.; Micikas, R. J. PCT Int. Appl. WO 2014177593 A1 20141106, 2014.

(14). Pettersen, E. F.; Goddard, T. D.; Huang, C. C.; Couch, G. S.; Greenblatt, D. M.; Meng, E. C.; Ferrin, T. E. *J. Comput. Chem.* **2004**, *25*, 1605-12.

(15). Trott, O.; Olson, A. J. *J. Comput. Chem.* **2010***, 31*, 455-461.

(16). Morris, G. M.; Huey, R.; Lindstrom, W.; Sanner, M. F.; Belew, R. K.; Goodsell, D. S.; Olson, A. J. *J. Comput. Chem.* **2009**, *30*, 2785–2789.

(17). Schmidt, M. W.; Baldridge, K. K.; Boatz, J. A.; Elbert, S. T.; Gordon, M. S.; Jensen, J. H.; Koseki, S.; Matsunaga, N.; Nguyen, K. A.; Su, S.; Windus, T. L.; Dupuis M.; Montgomery, J. *J. Comput. Chem.* **1993**, **14**, 1347–1363.

(18). Iannotti, F. A.; De Maio, F.; Panza, E.; Appendino, G.; Taglialatela-Scafati, O.; De Petrocellis, L.; Amodeo, P.; Vitale, R.M. *Molecules* **2020**, *25*, 1119.

(19). Fox, T.; Kollman, P.A. *J. Phys. Chem. B* **1998**, *102*, 8070–8079.

(20). Wang, J.; Wolf, R. M.; Caldwell, J. W.; Kollman, P. A.; Case, D. A. *J. Comput. Chem.* **2004**, *25*, 1157-1174.

Supporting Information. Additional computational data, 1D and 2D NMR spectra of the new amorfrutins; 1D NMR spectra of synthetic amorfrutins. This material is available free of charge via the Internet at http://pubs.acs.org.